Journal of Pharmaceutical and Medical Research
Print ISSN: 2663-1954
Online ISSN: 2663-1962
DOI: https://doi.org/10.61784/jpmr3087

NON-CONTACT HEALTH MONITORING SYSTEM BASED ON MILLIMETER-WAVE RADAR

XiangRui Tang, Qian Guo, Dong Shen*
School of Electronic and Information Engineering, Lanzhou Jiaotong University, Lanzhou 730070, Gansu, China.
**Corresponding Author: Dong Shen*

Abstract: With the expansion of the companion-animal market, animal protection, health management and harmonious coexistence between animals and humans have become increasingly important. The source project designs a portable embedded vital-sign monitoring system based on millimeter-wave radar. The system uses the IWR6843AOPEVM FMCW radar to collect raw physiological data, extracts heart-rate and respiration information through signal processing, displays the results on an OLED module, and transmits the data wirelessly to an upper computer such as a smartphone. Three domestic Doberman Pinschers were selected as test subjects, and heart-rate and respiration data were collected across daily states. Non-parametric testing, Spearman correlation, decision-tree classification, reliability analysis and validity analysis were used to evaluate the experimental data and product feedback. The condensed results show that the system has non-contact, real-time and portable monitoring advantages. Heart rate is the main basis for state classification, the decision-tree model performs well, and questionnaire analysis indicates that continuous working time and portability are the user concerns that require further optimization.
Keywords: Millimeter-wave radar; Vital-sign monitoring; Embedded system; Wireless transmission; Animal health; Decision tree; Questionnaire analysis

1 INTRODUCTION

Traditional vital-sign detection methods are often invasive, operationally complex, or unsuitable for long-term real-time monitoring. Millimeter-wave radar provides a non-contact alternative because it can sense small chest-wall motions related to respiration and heartbeat. The source document therefore applies millimeter-wave radar to animal vital-sign monitoring, with the aim of providing a real-time, accurate and comfortable detection scheme for animal health assessment. The system is also connected with broader application scenarios such as health management, animal behavior observation, safety warning and rescue support. Recent radar-based vital-sign and sensing studies also show that FMCW radar, mmWave SoCs, human activity recognition, multi-object tracking and posture or heart-rate estimation are active research directions[1-2].

The source project focuses on software algorithms and detection-system design. Because millimeter-wave signals are affected by multipath, clutter and noise, the signal-processing algorithm must extract reliable physiological signals from complex radar echoes. On the system side, the hardware and software must support real-time acquisition, display, wireless transmission and convenient interaction. The retained research content includes: the overall system scheme, hardware module design, ESP32 lower-computer software, radar signal processing, upper-computer interface, module debugging, animal data analysis, machine-learning classification and questionnaire-based product evaluation.

2 OVERALL SYSTEM DESIGN

The system uses ESP32_WROOM32 as the core control module and IWR6843AOPEVM as the millimeter-wave radar acquisition module. The radar collects raw physiological data, and the signal-processing algorithm converts the data into vital-sign information such as respiration and heart rate. The ESP32 module displays the processed data on the OLED screen, allows user interaction through a rotary encoder, and transmits the data to a smartphone upper-computer application through the wireless module. Figure 1 keeps the original overall design diagram extracted from the source Word file[3-5].

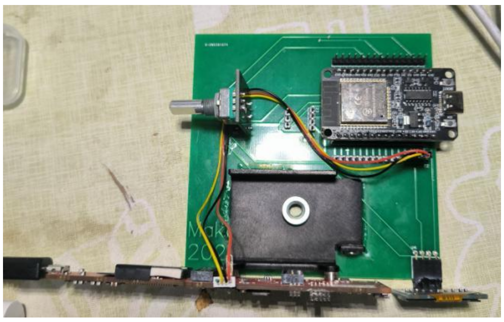

Figure 1 Overall Design Diagram

FreeRTOS is used to manage task scheduling and resource allocation, ensuring coordinated operation of radar acquisition, display refresh, encoder input and wireless communication. The original signal-processing flow shown in Figure 2 converts radar echoes into stable vital-sign outputs through filtering and frequency-domain analysis. The final product structure fixes key modules through PCB design, which improves wiring stability, reliability and system integration[6-8].

a) Slave address bit (SA0)
SSD1306 has to recognize the slave address before transmitting or receiving any information by the I^2C-bus. The device will respond to the slave address following by the slave address bit ("SA0" bit) and the read/write select bit ("R/W#" bit) with the following byte format,
b_7 b_6 b_5 b_4 b_3 b_2 b_1 b_0
0 1 1 1 1 0 SA0 R/W#
"SA0" bit provides an extension bit for the slave address. Either "0111100" or "0111101", can be selected as the slave address of SSD1306. D/C# pin acts as SA0 for slave address selection.
"R/W#" bit is used to determine the operation mode of the I^2C-bus interface. R/W#=1, it is in read mode. R/W#=0, it is in write mode.

Figure 2 Millimeter-Wave Radar Signal-Processing Flow

3 HARDWARE AND LOWER-COMPUTER DESIGN

The hardware consists of the millimeter-wave radar module, wireless module, rotary encoder, OLED display module and baseboard PCB. The radar module uses TI IWR6843AOPEVM. It contains an IWR6843AOP MCU, two micro-USB interfaces, CAN interfaces and an I2C interface. One micro-USB interface is used for power supply and another is used for serial communication. The IWR6843AOP integrates the radar sensor, radar-control part and DSP data-processing part. Figure 3 shows the radar module and its role in the embedded system.

Figure 3 IWR6843AOPEVM Millimeter-Wave Radar Module

The wireless module uses ESP32-related communication capability to transmit vital-sign data to a mobile upper computer. The rotary encoder module offers a convenient local control method for switching display states and user operations. The OLED display module is driven through I2C; in the source design, an 8 × 128 two-dimensional buffer is defined so that every bit corresponds to an OLED pixel. Continuous I2C transmission is then used to refresh the screen efficiently. The communication protocol sends frame head, respiration frequency, heart-rate frequency, checksum and frame tail bytes, so the lower computer and upper computer can parse data consistently[9-10].
The detailed communication-frame definition is summarized in Table 1, which specifies the frame head, respiration-frequency field, heart-rate-frequency field, checksum, and frame tail used for consistent lower-computer and upper-computer parsing.

Table 1 Communication Frame Structure

Frame head	Respiration frequency	Heart-rate frequency	Checksum	Frame tail
Byte	Byte	Byte	Byte	Byte
0xA5	0x	0x	0x	0x5A

The lower-computer software is divided into OLED display control, rotary encoder processing, communication protocol parsing and ring-buffer design. The OLED program defines character arrays and display functions to draw points, lines, rectangles and strings. The rotary encoder program detects rotation and button operations, while the communication program packages and parses heart-rate and respiration data. The ring array improves data buffering and prevents real-time data from being lost during asynchronous acquisition and display.

4 RADAR ALGORITHM AND SYSTEM DEBUGGING

The radar algorithm extracts respiratory and heartbeat signals from small periodic chest motions. In the source document, FFT and Kalman filtering are used to improve frequency-domain extraction and data stability. For a periodic vital-sign signal, frequency-domain analysis converts the time-domain sequence into a spectrum, making it possible to detect the respiration peak and heart-rate peak. This part is kept as a textual algorithm description because the source document does not provide an independent editable equation for this step.

For smoothing physiological measurements, the source text describes the use of Kalman filtering to improve the stability and reliability of the detected heart-rate and respiration data. Since the source does not list a separate Kalman update formula in this section, the condensed paper does not add one.

Module debugging in the source includes rotary encoder debugging, OLED display debugging, radar debugging and Bluetooth communication debugging. The OLED screen successfully displays respiratory and heart-rate values. The Bluetooth communication test verifies data transmission to the mobile upper computer, and the complete system test confirms that the radar, ESP32, display and wireless functions can operate together.

Figure 4 shows the OLED display and Bluetooth communication test, and Figure 5 presents the integrated product test after module assembly.

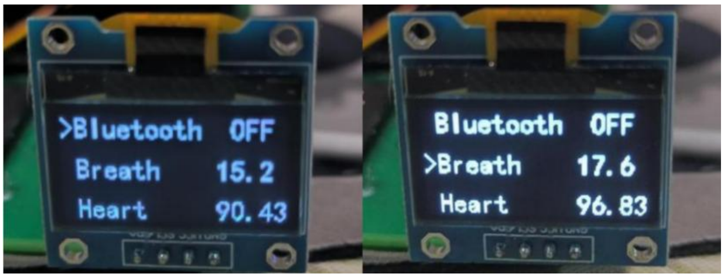

Figure 4 OLED Display and Bluetooth Communication Test

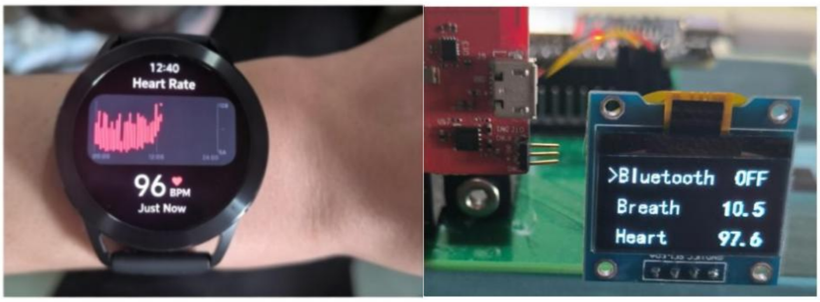

Figure 5 Integrated Product Test

5 ANIMAL DATA COLLECTION AND STATISTICAL ANALYSIS

Three domestic Doberman Pinschers were used as test subjects. Heart-rate and respiration data across a day were collected and matched with animal states, forming three groups of experimental data. Because the data are not normally distributed, the source uses non-parametric testing. The Friedman test is introduced to compare whether multiple related groups differ significantly. If k samples and b blocks are considered, the Friedman statistic can be written as

$$Q=\frac{12}{bk(k+1)}\sum R_i^2-3b(k+1) \tag{1}$$

Normality testing shows that the S-W significance values of the three heart-rate groups are 0.000***, so normality is rejected. The respiration groups also reject normality. The source therefore uses the Friedman test. Table 2 compresses the key non-parametric results.

Table 2 Friedman Test Results for Heart Rate and Respiration

Indicator	Group	Sample size	Median	Standard deviation	Statistic	P	Effect value
Heart rate	Group 1	288	70.5	19.58	4.292	0.117	0.035
Heart rate	Group 2	288	69.95	19.526	4.292	0.117	0.035
Heart rate	Group 3	288	69.5	20.767	4.292	0.117	0.035
Respiration	Group 1	288	25.6	7.09	9.934	0.007***	0.049
Respiration	Group 2	288	25.4	8.4	9.934	0.007***	0.049
Respiration	Group 3	288	24.35	8.751	9.934	0.007***	0.049

Spearman correlation is then used to determine whether heart rate and respiration reflect the dog's state. If two rank sequences are X and Y, and di denotes the rank difference of the i-th paired observation, the Spearman coefficient is

$$r_s=1-\frac{6\sum d_i^2}{n(n^2-1)} \quad (2)$$

The resulting correlation coefficients are reported in Table 3, showing the relationships among heart rate, respiration, and animal state before the heat-map visualization is interpreted.

Table 3 Spearman Correlation Coefficients

Variable	Heart rate	Respiration	State
Heart rate	1(0.000***)	0.892(0.000***)	0.452(0.000***)
Respiration	0.892(0.000***)	1(0.000***)	0.247(0.000***)
State	0.452(0.000***)	0.247(0.000***)	1(0.000***)

As shown in Figure 6, the correlation heat map indicates that the correlation between heart rate and state is 0.452, while the correlation between respiration and state is 0.247. Therefore, both indicators are related to the animal state, and heart rate is the stronger classification basis.

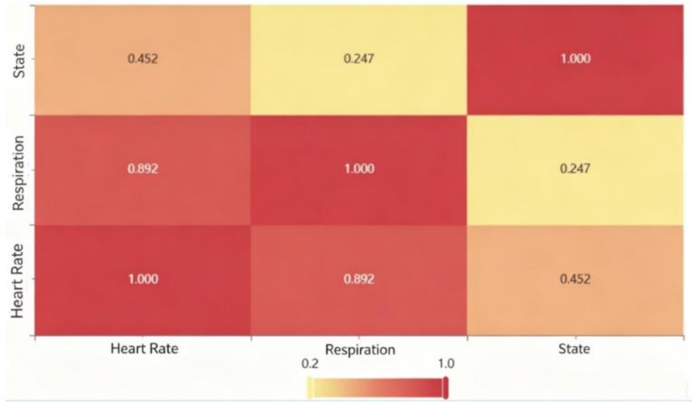

Figure 6 Correlation Heat Map

6 DECISION-TREE CLASSIFICATION MODEL

The source uses a CART decision-tree model to predict Doberman states. The decision tree recursively builds a tree structure from the top down, using feature tests at internal nodes and class labels or class distributions at leaf nodes. The original text describes information entropy and information gain as the basis for measuring uncertainty reduction. Entropy is expressed as

$$H(D)=-\sum p_i log p_i \quad (3)$$

where p_i is the probability of class i in dataset D. The classifier is trained with SPSSPRO, using a 0.7 data split, no data shuffling, no cross-validation, gini as the split evaluation criterion, and best as the feature split-point selection standard. Table 4 keeps the model performance results from the source.

Figure 7 presents a newly redrawn decision-tree classification result with clearer node spacing and without visual obstruction, making the heart-rate-dominant splitting structure easier to read.

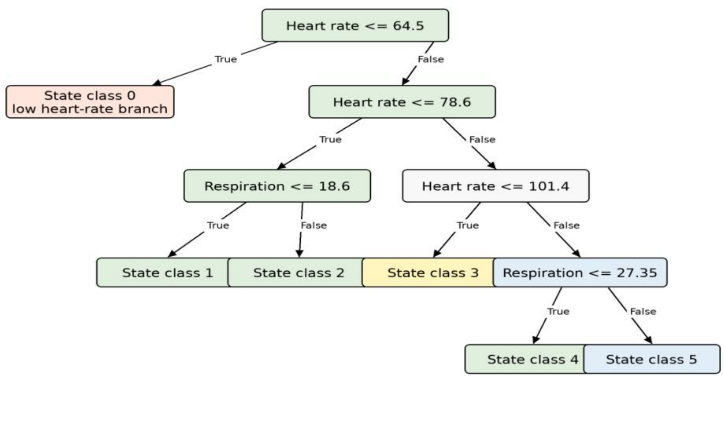

Redrawn decision-tree structure based on the source result; heart rate is the dominant split variable.

Figure 7 Decision-Tree Classification Result (Redrawn for Clarity)

Table 4 Decision-Tree Classification Performance

Dataset	Accuracy	Recall	Precision	F1
Training set	0.94	0.94	0.939	0.931
Test set	0.938	0.938	0.94	0.933

The training and test metrics are all close to 1, indicating that the classifier performs well on the collected data. The source further states that the classification result mainly depends on heart rate, which is consistent with the correlation analysis.

7 QUESTIONNAIRE EVALUATION AND APPLICATION VALUE

After the product is put into use, the source carries out a questionnaire survey. Reliability analysis is used to evaluate whether the scale is stable and consistent. Cronbach's alpha is the main reliability indicator, and the source formula is retained as

$$\alpha=\frac{k}{k-1}(1-\frac{\sum S_i^2}{S_t^2}) \tag{4}$$

where k is the number of items, Si2 is the variance of item i, and St2 is the variance of the total score. The questionnaire has a Cronbach's alpha coefficient of 0.738 and a standardized Cronbach's alpha coefficient of 0.723, with 7 items and 100 samples, indicating acceptable reliability. Validity analysis gives KMO=0.797 and Bartlett P=0.000***, so factor analysis is valid. The source indicates that continuous working time and environmental adaptability receive stronger customer attention, while multiple-response analysis shows that portability and continuous working time need further improvement compared with traditional detection bracelets.
Figure 8 visualizes the questionnaire reliability result, supporting the interpretation that the scale has acceptable internal consistency (Table 5).

Table 5 Reliability and Validity Results

Analysis	Key value	Interpretation
Cronbach's alpha	0.738	The questionnaire reliability is acceptable
Standardized alpha	0.723	The standardized reliability result is acceptable
KMO	0.797	Factor analysis is applicable
Bartlett P	0.000***	Variables are correlated and validity analysis is meaningful
Main user concern	Portability and continuous working time	The system should be optimized in these directions

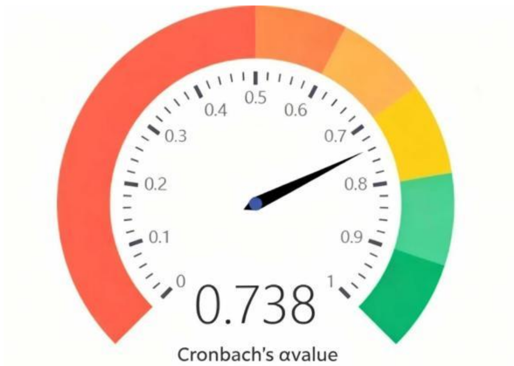

Figure 8 Reliability Result of the Questionnaire

The system has practical value in animal health monitoring, medical assistance, safety protection and rescue. It can monitor physiological parameters such as heart rate and respiration in a non-contact manner, avoid discomfort caused by contact sensors, and reduce infection risks. For animal care, the system can identify abnormal activity and support health warning. In rescue scenarios, the same vital-sign detection principle can help locate trapped individuals and provide useful physiological information.

8 CONCLUSION

The source project successfully designs and implements a millimeter-wave-radar-based animal vital-sign monitoring system. The system combines the IWR6843AOPEVM radar, ESP32 module, OLED display, rotary encoder and wireless communication module to realize non-contact physiological data acquisition, local display and mobile upper-computer monitoring. The animal experiment with three Doberman Pinschers shows that heart rate and respiration can be collected and associated with animal states. Non-parametric testing supports the rationality of the data analysis, Spearman correlation confirms that heart rate and respiration are related to state, and the decision-tree classifier achieves high accuracy, recall, precision and F1 values. Questionnaire analysis shows acceptable reliability and validity, while portability and continuous working time remain important optimization directions. Future work should improve anti-interference ability, enhance algorithm adaptability, support multi-target monitoring and promote product-oriented application in pet care, sports health and animal safety management.

COMPETING INTERESTS

The authors have no relevant financial or non-financial interests to disclose.

REFERENCES

[1] Mallat N K, Ishtiaq M, Rehman A U, et al. Millimeter-Wave in the Face of 5G Communication Potential Applications. IETE Journal of Research, 2022, 68(4): 2522-2530.
[2] Liu B, Ma K X, Fu H P, et al. Recent Progress of Silicon-Based Millimeter-Wave SoCs for Short-Range Radar Imaging and Sensing. IEEE Transactions on Circuits and Systems II: Express Briefs, 2022, 69(6): 2667-2671.
[3] Yu C X, Xu Z Z, Yan K, et al. Noninvasive Human Activity Recognition Using Millimeter-Wave Radar. IEEE Systems Journal, 2022, 16(2): 3036-3047.
[4] Wu J C, Dahnoun N. A health monitoring system with posture estimation and heart-rate detection based on millimeter-wave radar. Microprocessors and Microsystems, 2022, 94: 104681.
[5] Mao T, Zhang Y, Zhu K Q, et al. Estimation of human gait features by trajectory tracking and recombination using radar range-Doppler-time data. IET Radar, Sonar & Navigation, 2023, 17(2): 236-246.
[6] Pearce A, Zhang J A, Xu R C, et al. Multi-Object Tracking with mmWave Radar: A Review. Electronics, 2023, 12(2): 308.
[7] Zhao W, Zhang J K, Zhang X P, et al. Multiple-Target Localization by Millimeter-Wave Radars With Trapezoid Virtual Antenna Arrays. IEEE Internet of Things Journal, 2022, 9(20): 19589-19598.
[8] Yang B, Zhang H, Chen Y R, et al. Urban Traffic Imaging Using Millimeter-Wave Radar. Remote Sensing, 2022, 14(21): 5354.
[9] Gan Y D, Zheng L, Zhang Z D, et al. Multi-target detection and tracking based on fusion of millimeter-wave radar and depth vision. Automotive Engineering, 2021, 43(7): 1022-1029, 1056.
[10] Wu J Y, Zhu Z Y, Wang H P. Human Detection and Action Classification Based on Millimeter Wave Radar Point Cloud Imaging Technology. Journal of Physics: Conference Series, 2021, 2029(1): 012054.